Development of Active and Stable Low Nickel Content Catalysts for Dry Reforming of Methane

Quan Luu Manh Ha [1,2], Udo Armbruster [1],*, Hanan Atia [1], Matthias Schneider [1], Henrik Lund [1], Giovanni Agostini [1], Jörg Radnik [3], Huyen Thanh Vuong [1] and Andreas Martin [1]

[1] Department Heterogeneous Catalytic Processes, Leibniz-Institut für Katalyse e.V.,
Albert-Einstein-Str. 29a, 18059 Rostock, Germany; quan.ha@catalysis.de (Q.L.M.H.);
hanan.atia@catalysis.de (H.A.); matthias.schneider@catalysis.de (M.S.);
henrik.lund@catalysis.de (H.L.); giovanni.agostini@catalysis.de (G.A.);
huyen.vuong@catalysis.de (H.T.V.); andreas.martin@catalysis.de (A.M.)
[2] Vietnam Petroleum Institute, 167 Trung Kinh, Cau Giay, Hanoi 100000, Vietnam
[3] Division 6.1, Surface Analysis and Interfacial Chemistry, Federal Institute for Materials Research and Testing,
Richard-Willstätter-Str. 12, 12489 Berlin, Germany; joerg.radnik@bam.de
* Correspondence: udo.armbruster@catalysis.de; Tel.: +49-381-1281-257

Abstract: Methane dry reforming (DRM) was investigated over highly active Ni catalysts with low metal content (2.5 wt %) supported on Mg-Al mixed oxide. The aim was to minimize carbon deposition and metal sites agglomeration on the working catalyst which are known to cause catalyst deactivation. The solids were characterized using N_2 adsorption, X-ray diffraction, temperature-programmed reduction, X-ray photoelectron spectroscopy, and UV-Vis diffuse reflectance spectroscopy. The results showed that $MgO-Al_2O_3$ solid solution phases are obtained when calcining Mg-Al hydrotalcite precursor in the temperature range of 550–800 °C. Such phases contribute to the high activity of catalysts with low Ni content even at low temperature (500 °C). Modifying the catalyst preparation with citric acid significantly slows the coking rate and reduces the size of large octahedrally coordinated NiO-like domains, which may easily agglomerate on the surface during DRM. The most effective Ni catalyst shows a stable DRM course over 60 h at high weight hourly space velocity with very low coke deposition. This is a promising result for considering such catalyst systems for further development of an industrial DRM technology.

Keywords: dry reforming of methane; carbon dioxide; nickel; $MgO-Al_2O_3$ solid solution

1. Introduction

The dry reforming of methane (DRM), which is the strong endothermic reaction of methane with carbon dioxide to syngas (Equation (1)), has gained increasing interest in recent years:

$$CH_4 + CO_2 \rightarrow 2CO + 2H_2 \tag{1}$$

This reaction cannot only be effectively applied for natural gas conversion into liquid fuels via the syngas route, but also may contribute to reducing the emission of CO_2 and CH_4 greenhouse gases to our atmosphere [1–4]. The syngas from DRM with a low ratio of H_2/CO is suitable for subsequent syntheses of oxygenated chemicals [5] and hydrocarbons via the Fischer-Tropsch synthesis [6]. However, DRM requires a high reaction temperature [7]. This leads to several catalyst deactivation processes resulting in catalytic sites' agglomeration and coke formation [8]. The deposited carbon is formed during the DRM reaction through CH_4 decomposition (Equation (2)) and Boudouard (Equation (3)) reactions [4,9,10]:

$$CH_4 \rightarrow C + 2H_2 \tag{2}$$

$$2CO \rightarrow CO_2 + C \tag{3}$$

Therefore, the great challenge for the development of a DRM process is the development of catalysts with high activity for the conversion of CO_2 and CH_4 and strong ability in suppressing the formation of carbon deposits [8]. Ni based catalysts were most frequently reported in DRM studies due to their high activity, availability, and lower price compared to other transition and noble metals [11–13]. In those studies, efforts were focused on improving the activity and stability of Ni active sites in the following aspects: screening and modifying the properties of the support, selecting the support and catalyst preparation methods, and the addition of promoters [13].

Suitable supports play a key role in the enhancement of catalytic activity and the suppression of carbon deposition for the DRM reaction [4]. γ-Al_2O_3 has been widely employed as a support for DRM catalysts because of its high availability and low price [4,14]. It was also suggested that an improvement of the support properties for the adsorption and activation of CO_2 would accelerate the gasification of the deposited carbons and prevent the rapid deactivation of the catalyst [13]. In order to achieve that, certain alkaline-earth metal oxides were incorporated into alumina to increase the basicity of the support [13]. MgO was reported to improve the catalytic performance of Ni/Al_2O_3 because of the strong interaction between Ni and the supports and the basic property of the metal oxide could suppress carbon formation in the dry reforming process [15,16]. The cooperation of Mg and Al oxides in same support material can result in many structures, such as $MgAl_2O_4$ spinel, which is the well-studied support structure for Ni catalysts in several types of reactions due to its good chemical stability and mechanical strength [13,17]. Other structures of MgO and Al_2O_3 mixed oxides could also serve as supports for DRM catalysts in order to disperse and stabilize the metallic Ni species and promote the coking resistance behavior [18–20]. However, only a few DRM studies have focused on low Ni content catalysts with such mixed oxide supports, probably due to the partial formation of stable but poorly active phases, such as $NiAl_2O_4$ spinel or NiO-MgO solid solution [17]. However, Ni catalysts with low metal content are potentially one of the solutions for overcoming the abovementioned problems of DRM. This is due to higher catalyst stability and lower carbon deposition achieved by forming highly dispersed and smaller sized Ni particles [21,22].

Chelating agents are molecules with two or more electron-pair donor atoms which can act as a ligand and attach themselves to metal ions [23]. This causes the formation of metal complexes, which were also studied to modify the preparation route for supported catalysts using the impregnation method [23]. In such studies, uniform distribution and high dispersion of the active component over the support were achieved. Those beneficial properties arise from the diffusion-controlled homogeneous distribution of metal atoms in the precursor structure as well as the enhanced viscosity of the gel-like material inhibiting redistribution of the impregnated species during subsequent drying. Citric acid (CA) is the most common and promising compound among the chelating agents because it is cheap, highly soluble, and environmentally harmless [24].

The aim of this study is to explore the potential of catalysts with low Ni content, according to the literature review [8], on Mg-Al mixed oxide supports (Mg-Al) that can be both stable and active in DRM at high weight hourly space velocity (WHSV). Modifications of the support and catalyst preparation were investigated to enhance the stability of the catalyst without deteriorating the DRM activity. Thus, various Ni catalysts with different supports were prepared via modified routes and tested in a continuous fixed bed reactor. Long-term experiments together with the characterization of fresh and spent catalysts using various techniques, including inductively coupled plasma-optical emission spectroscopy and atomic adsorption spectroscopy (ICP-OES resp. AAS), N_2 physisorption, X-ray powder diffraction (XRD), X-ray photoelectron spectroscopy (XPS), Temperature-programmed reduction (TPR), and UV-Vis diffuse reflectance spectroscopy (UV-Vis-DRS), indicated important attributes that contribute to catalyst activity and stability.

2. Results

2.1. Characterization of the Catalysts

First of all, the crystalline structures of the supports and catalysts can be revealed by X-ray diffraction. Figure 1 depicts the XRD patterns of $MgO \cdot Al_2O_3$ mixed oxides (denoted as Mg.Al.X with X indicating the calcination temperature) obtained from hydrotalcite material with different calcination temperatures (550, 700, 800, 1000 °C). The patterns of MgO and Al.550 (boehmite calcined at 550 °C) are also displayed as references. When hydrotalcite samples are calcined at temperatures between 550 °C and 800 °C, the XRD patterns of the resulting Mg.Al.X samples show broad reflections at about $2\theta = 43°$ and 63° which have 2θ values higher than those of periclase (cubic form of magnesium oxide, ICDD (International Centre for Diffraction Data) file No. 01-071-1176) but lower than those of γ-Al_2O_3 (ICDD file No. 00-010-0425). The patterns of periclase and γ-Al_2O_3 structures are clearly observed in MgO and Al.550 samples, respectively. This highlights the incorporation of smaller Al^{3+} cations into the bulk of the periclase (MgO) structure lattice, establishing a solid solution between MgO and Al_2O_3 (Mg-Al-O) [25,26]. A higher calcination temperature modifies such an incorporation which can be observed as a shift of reflections to lower 2θ values. Up to 800 °C, the pattern of such a solid solution is still observable. Besides, Mg.Al.700 and Mg.Al.800 show reflections ($2\theta = 31.3°$; 37°; 45°; 55.5°; 59°; 65°) assigned to the formation of the $MgAl_2O_4$ phase (ICDD file No. 00-021-1152) at higher calcination temperatures [27]. At 1000 °C, no reflection of the solid solution can be observed while peaks assigned to periclase MgO and $MgAl_2O_4$ phases are sharp and characteristic, indicating the high crystallinity of those phases. Those results are in accordance with other studies [25,28,29] focusing on the thermal decomposition behavior of hydrotalcite, producing Mg-Al oxides and mixed oxides in solid solution or spinel structures, particularly when a low heating rate was applied.
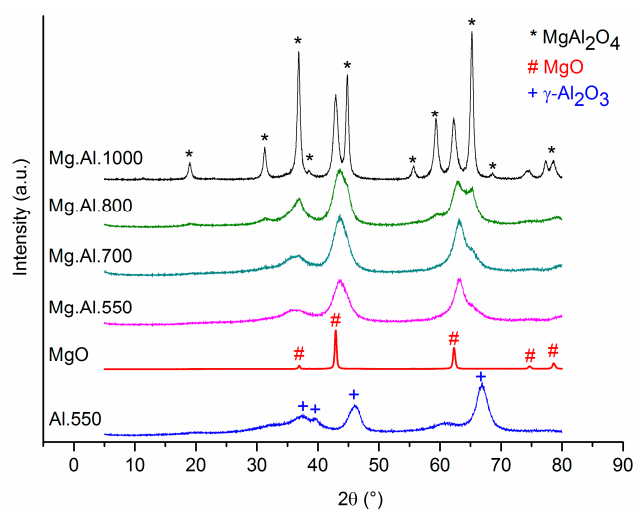

Figure 1. XRD patterns of the MgO, γ-Al_2O_3, and Mg.Al supports.

The XRD patterns of impregnated low content Ni samples (not shown) show no significant differences from those of their corresponding supports. This reflects the formation of well-dispersed Ni^{2+} species leading to very small Ni particles that were not detected by the XRD measurements [30,31]. This might be also due to Ni diffusion into the bulk of the supports, especially when a high calcination temperature was applied during the preparation [31].

The XRD patterns of spent Ni catalysts are presented in Figure 2. Ni metal species (Ni^0), which are the result of the pre-reduction process before DRM, can be detected with reflections at $2\theta = 44.5°$ and 51.8° (ICDD file No. 01-071-3740). Spent Ni/Al.550 (Figure 2b) shows a pattern with additional reflections at the mentioned 2θ values compared to the fresh one. This is assigned to the formation of highly crystalline Ni^0 domains due to agglomeration during the reaction. On the other hand, the XRD

pattern of spent Ni/Mg.Al.550 (Figure 2a) displays a similar profile as the fresh sample, proving the stability of the material during the reaction. This result is probably due to the incorporation of Ni into the solid solution or/and the $MgAl_2O_4$ spinel framework since such stable phases prevent the structural transformation at the high reaction temperature [17,18,21].
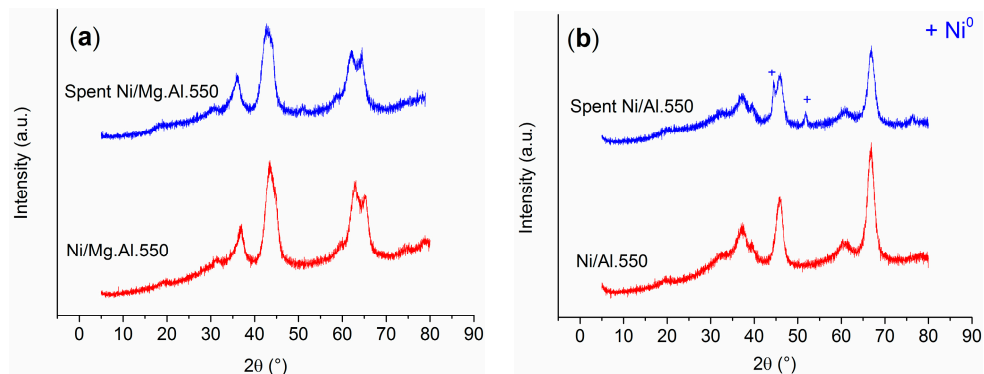

Figure 2. XRD patterns of fresh and spent samples of Ni supported (**a**) on Mg.Al.550 and (**b**) on Al_2O_3 (DRM (dry reforming of methane) conditions: 700 °C, 1 bar, CH_4:CO_2 = 1, WHSV (weight hourly space velocity) = 85 L/(g_{cat} × h), TOS (time-on stream) = 8 h).

The N_2 adsorption-desorption isotherms together with the BJH (Barrett-Joyner-Halenda) pore size distributions (PSD) of the Mg.Al.550.800 support and corresponding Ni catalysts are shown in Figures 3 and 4, respectively. All isotherms exhibit type II curves with H3 type hysteresis loops according to the IUPAC (International Union of Pure and Applied Chemistry) classification, which reflects the contribution of the mesopores in the materials.
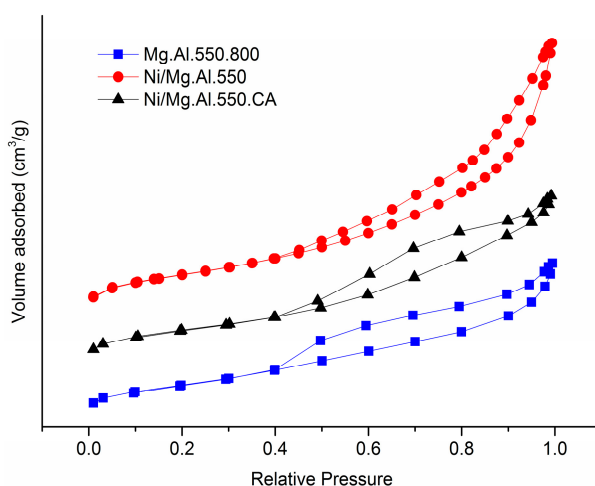
Figure 3. N_2 physisorption isotherms of fresh catalysts and their support Mg.Al.550.800.

Regarding the pore size distribution (Figure 4), both the Ni samples show a shift toward higher pore diameter compared to their support. This feature most likely indicates the re-structuring of the support material in the impregnation step. However, in both cases, no limitation by internal diffusion is expected for the feed molecules, which are small compared to the size of the pores.
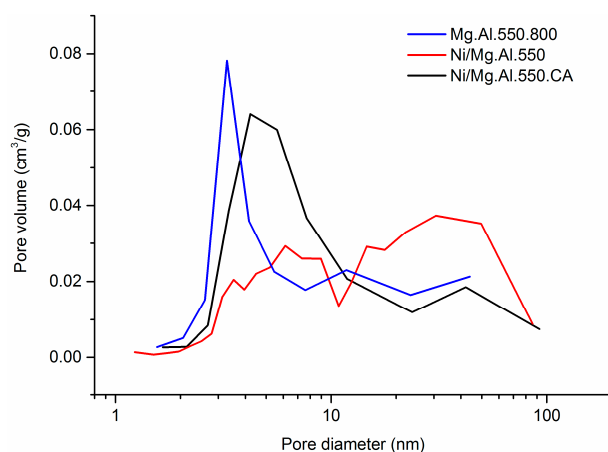
Figure 4. Pore size distribution of fresh catalysts and their support Mg.Al.550.800.

The textural parameters of the calcined Ni samples and the supports are summarized in Table 1.

Table 1. Textural properties of calcined catalysts and their supports.

| Catalyst	S_{BET} (m^2/g)	Total Pore Volume (cm^3/g)
Mg.Al.550	180	0.24
Mg.Al.550.800 [1]	147	0.24
Mg.Al.1000	85	0.37
Al.550	234	0.54
MgO	50	0.35
Ni/Mg.Al.550	174	0.40
Ni/Mg.Al.550.CA [2]	156	0.27
Ni/Mg.Al.1000	82	0.36
Ni/Al.550	178	0.47
Ni/MgO	45	0.33

[1] Mg.Al.550 calcined again at 800 °C; [2] Citric acid was used during impregnation.

While all bare supports were calcined once at 550 °C and the resulting catalysts at 800 °C, one particular sample denoted as Mg.Al.550.800 was calcined at 550 and 800 °C as a reference support without impregnation.

Support Al.550 displays the highest surface area and pore volume among the studied supports. However, Ni/Mg.Al.550 and Ni/Al.550 show similar texture parameters. Both Ni/Mg.Al.550 and Ni/Mg.Al.550.CA expose larger surface areas than their corresponding support (Mg.Al.550.800) which might be explained by the mentioned re-structuring of the support surface due to the dissolution of alumina and magnesia into the acidic solution (containing Ni^{2+} and/or citric acid) during the impregnation step [30]. Ni/Mg.Al.1000 possesses relatively low surface area because its support was calcined at high temperature. Ni/Al.550 and Ni/MgO show textural parameters which are in agreement with their supports' attributes.

The reducibility of the materials was examined by TPR measurements. It should be noted that Ni^{2+} species are the predominant reducible ones in those samples. The TPR profile of the unsupported NiO sample as the reference is exhibited in Figure 5 with an intense peak at 350 °C, illustrating the bulk NiO reduction. Generally, all studied supported Ni samples display poor reducibility, possibly due to their low Ni loading and high sample calcination temperature. Those effects might cause strong interaction of Ni^{2+} and the support, suppressing free NiO that can otherwise easily react with hydrogen [32,33]. On Al$_2$O$_3$, the Ni^{2+} species show high-temperature reduction peaks at 700 °C and the reduction is incomplete below 1000 °C (Figure 5). This behavior is typical for the reduction of nickel aluminate species. The mentioned samples were prepared at high calcination temperature

(800 °C) and low Ni content (2.5 wt %), leading to unavoidable poor reducibility due to the diffusion of Ni^{2+} into the Al_2O_3 lattice, suppressing the formation of bulk NiO species [34]. The TPR profile of Ni/MgO discloses peaks at somewhat lower temperatures mainly assigned to the reduction of Ni^{2+} species in the outer face or subsurface layers of the MgO lattice. The remaining shoulder at higher temperature of the profile is related to the reduction of the species in solid solution, resulting from the diffusion of Ni^{2+} species into the periclase lattice due to high calcination temperature (800 °C) [32]. Ni/Mg.Al.550 shows a broad peak starting at 600 °C, reflecting the reduction of Ni^{2+} species mainly in the solid solution [35] and/or in the spinel structure when Ni is embedded in Mg and Al mixed oxides prepared from the hydrotalcite precursor [36]. The reducibility of that sample is slightly better than that for Ni/MgO or Ni/Al.550. Indeed, Ni/Mg.Al.550 displays a weak band at 500 °C in its TPR profile, attributed to the reduction of NiO species formed on the surface that have weak interaction with the support [37]. Additionally, it shows higher H_2 consumption than the single oxide supported samples (Table 2). This is similar to literature reports [20] concluding that the availability of Mg in Ni-Al containing samples facilitates the solid solution formation and stabilizes the Ni species on the surface. This benefit avoids the Ni diffusion into the alumina lattice, and therefore suppresses the formation of the poorly reducible $NiAl_2O_4$ spinel structure.
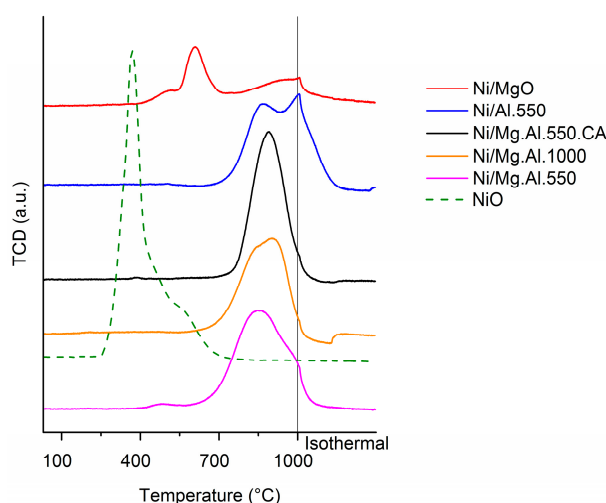
Figure 5. TPR (temperature-programmed reduction) profiles of several supported Ni catalysts and NiO.

In comparison to Ni/Mg.Al.550, both Ni/Mg.Al.550.CA and Ni/Mg.Al.1000 show a shift in reduction peak maxima in their TPR profiles to higher temperature (900 °C) (Figure 5). Besides, they consume less hydrogen in the TPR experiment (Table 2), illustrating the formation of poorly reducible Ni^{2+} species that have higher interaction with the support frameworks [35,38].

Table 2. H_2 consumption in TPR for the catalysts.

Sample	H_2 Consumption (μmol/g)
Ni/Al.550	397
Ni/MgO	181
Ni/Mg.Al.550	480
Ni/Mg.Al.1000	404
Ni/Mg.Al.550.CA	437

XPS measurements were carried out to characterize the surface composition of the materials. The binding energy (BE) values were also measured to verify the oxidation states of the atoms as well as their chemical and physical environments. All of the samples show binding energies (BE) corresponding to the Ni $2p_{3/2}$ region within the range around 855–857 eV (Table 3) [39]. Those are

slightly higher than the values for free NiO (854.5 eV) [39,40] and close to that observed for Ni_2O_3 (856 eV) [35,39], $NiAl_2O_4$ (856 eV) [35,39], NiO-MgO solution (855.7 eV [40] or 856 eV [41]), and solid solution Mg(Ni.Al)O (855.5 eV) [35].

Table 3. XPS (X-ray photoelectron spectroscopy) and ICP-AES (Inductively coupled plasma atomic emission spectroscopy) results for the catalysts.

Sample	Binding Energy (eV)	Surface Molar Ratio [1]		Bulk Molar Ratio [2]	
	Ni 2p$_{3/2}$	Ni/(Mg + Al)	Mg/Al	Ni/(Mg + Al)	Mg/Al
Ni/Al.550	855.5	0.029	-	0.022	0
Ni/MgO	-[3]	-[3]	-[3]	0.017	-
Ni/Mg.Al.550	856.9	0.063	0.4	0.019	1.3
Ni/Mg.Al.1000	856.1	0.057	0.3	0.019	1.3
Ni/Mg.Al.550.CA	855.2	0.071	1.6	0.019	1.3
Mg.Al.550	-	-	1.2	-	1.3
Mg.Al.550.800	-	-	1.1	-	1.3
Mg.Al.1000	-	-	1.5	-	1.3

[1] XPS results; [2] ICP results; [3] Ni content is below the XPS detection limit.

In any case, it could be suggested that the transfer of electrons from nickel to electron-poor magnesium and/or aluminum species in the structure causes the BE to shift to a higher value than that of free NiO [35]. Those results indicate a strong interaction of Ni with the supports, as seen in the TPR results, lowering their reducibility compared to pure NiO (Figure 5).

Regarding the Mg/Al surface ratio (Table 3) of samples with the Mg.Al support, there are differences between the Ni catalysts and their corresponding supports, suggesting the mentioned alumina and magnesia dissolution and re-dispersion of the surface components after preparation in some cases. On one side, impregnating Ni^{2+} onto the support in the presence of CA slightly increases the Mg/Al ratio from 1.1 to 1.6, but still maintains the Mg-rich surface. On the other hand, Ni/Mg.Al.550 and Ni/Mg.Al.1000 show Al-rich surfaces. Those observations are not fully understood, but are probably due to the Mg and Al leaching rate and re-dispersion in different precursor solutions during catalyst preparation. However, the surface Ni concentrations of those samples are still comparable.

Comparison of the surface Ni/(Mg + Al) ratio (from XPS) and bulk composition (from ICP) (Table 3) highlights the preferred location of Ni in different supports. Regarding the reference samples, Ni/MgO exposes almost no Ni on the surface and Ni/Al.550 shows a slightly higher surface Ni/(Mg + Al) ratio (0.029) compared to the bulk values (0.022). On the other hand, Ni/Mg.Al.550, Ni/Mg.Al.1000, and Ni/Mg.Al.550.CA expose Ni on the surface with significantly higher atom ratios (0.063, 0.057, and 0.071) compared to their bulk values (0.017–0.019). These data reflect the ability of Mg.Al supports to augment active Ni species on the outer shell of materials. Such an effect contributes to the higher reducibility of the Mg.Al supported samples compared to Ni/MgO and Ni/Al.550, as shown in the TPR profiles (Figure 5). Increasing the support calcination temperature from 550 to 1000 °C produces samples with less Ni^{2+} domains on the surface available for reduction [38]. As a result, Ni/Mg.Al.1000 provides poorer reducibility compared to Ni/Mg.Al.550 (Figure 5). This illustrates the ability of the Mg.Al.550 support with Mg-Al-O solid solution domains to enrich the surface Ni species and thus to enhance sample reducibility.

Introduction of CA during preparation increases the fraction of surface Ni^{2+} species. However, the reducibility of Ni/Mg.Al.550.CA as mentioned is not as high as that of Ni/Mg.Al.550 (Figure 5). The sample shows a sharp and symmetric reduction peak with a maximum temperature around 900 °C. These observations suggest that the low reducibility of Ni/Mg.Al.550.CA is primarily due to the higher dispersion of Ni species on the support surface [23], leading to a strong interaction with the Mg.Al material.

The coordination of the nickel (mostly Ni^{2+}) species in the samples was examined by UV-Vis-DRS (Diffuse reflection spectroscopy). This technique is helpful for the identification of the nickel phases. No absorption can be seen in the support samples (not shown), suggesting that only Ni^{2+} species are sensitive at the chosen analysis conditions. The UV-Vis-DRS spectra of the Ni impregnated samples on different supports are shown in Figure 6. Those spectra show intense signals in the UV region of 250–350 nm, which relate to the $O^{2-} \rightarrow Ni^{2+}$ charge transfer (CT) in the octahedral NiO lattice [42]. NiO shows strong absorption over the whole mentioned range which can be assigned to nonstoichiometric NiO containing some Ni^{3+} domains [42]. Mg.Al supported samples show shoulders in the range of 250–350 nm which cannot be found in the spectra of Ni/MgO and Ni/Al.550, suggesting weaker interaction of Ni species with the Mg.Al supports [30]. In comparison to Ni/Mg.Al.550.CA and Ni/Mg.Al.1000, a red-shift of the CT band of NiO is observed for Ni/Mg.Al.550, which points to the weakest interaction of Ni species and support among the studied samples. This explains the TPR results, which proved that Ni/Mg.Al.550.CA and Ni/Mg.Al.1000 have lower reducibility compared to Ni/Mg.Al.550 (Figure 5).
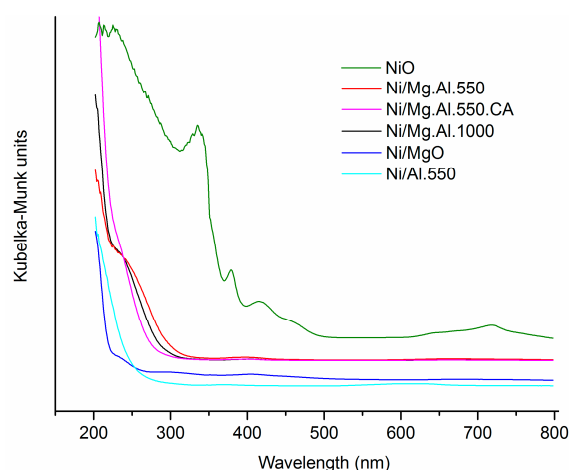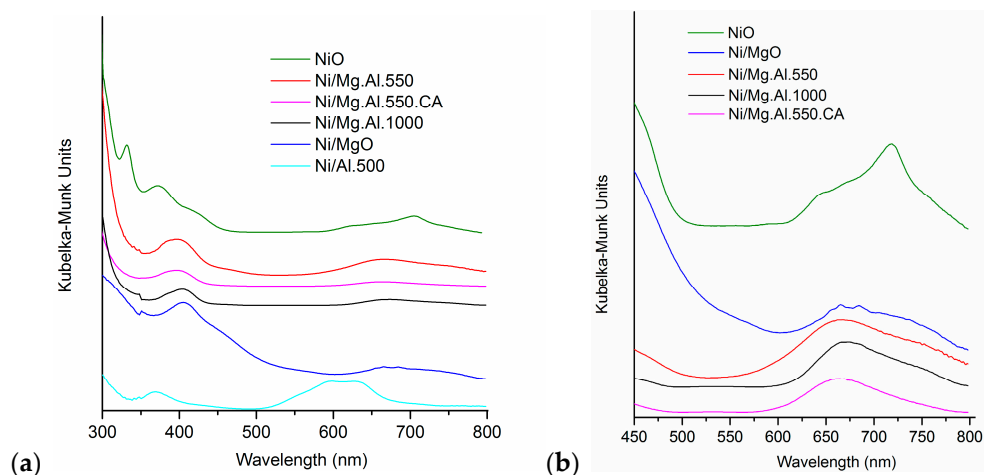

Figure 6. UV-Vis-DRS spectra of supported Ni catalysts and NiO.

A magnification of the UV-Vis-DRS spectra in the visible region (350–800 nm) of the mentioned samples can be seen in Figure 7. The signals in this region represent d-d transitions of Ni^{2+} ions mainly in octahedral (O_h) and tetrahedral coordination (T_d) [43]. Pure NiO presents intense signals at 380, 420, and 720 nm which illustrate the Ni^{2+} (O_h) in the cubic (rock-salt) NiO lattice [44]. Ni/Al.550, on the other hand, shows a doublet signal at 600–650 nm which is related to the Ni^{2+} (T_d) species in the nickel aluminate spinel lattice [44,45]. Besides, small absorption bands at 380 nm can be assigned to Ni^{2+} (O_h) in the $NiAl_2O_4$ spinel [46]. Ni/MgO displays a spectrum similar to that of the pure NiO sample. It shows an intense signal at 410 nm and a wide band at 650–800 nm which suggests a majority of Ni^{2+} (O_h) species. Those bands belong to the solid solution of Ni and Mg when Ni species migrate into the MgO parent lattice, which has a cubic rock-salt structure as well [47]. The absence of intense signals at 380 nm and 720 nm is probably due to the lack of bulk NiO in Ni/MgO [46]. This suggestion is supported by the XRD pattern of Ni/MgO (not shown), in which no crystalline structure other than periclase MgO can be seen. Indeed, the low content of Ni in the sample and the strong interaction between NiO and MgO results in the high dispersion of Ni species, thus suppressing the agglomeration of NiO in the calcination process. Ni/Mg.Al.550 shows a wide band from 380 nm to 410 nm with the highest intensity at around 400 nm, which is located between the corresponding signals of Ni/MgO and Ni/Al.550. This reveals the formation of octahedral coordination of the Ni domains which diffuse into the support framework of the solid solution Mg-Al-O. This kind of structure containing the three elements was also discussed in other studies [29,48] in which Ni^{2+} and Al^{3+} were substituted for the Mg^{2+} site in the parent MgO (periclase) structure (denoted as Mg(Ni,Al)O). Furthermore, it should

be noted that the presence of Ni^{2+} (O_h) in the $NiAl_2O_4$ spinel can be stated for the Ni/Mg.Al.550 sample. In [30], the authors claimed the formation of Ni^{2+} (O_h) species in $NiAl_2O_4$-like "surface spinel", identified by bands in the range of 405–410 nm. These surface spinel species were suggested to more likely exist in the samples with higher nickel content on the surface, similar to the surface features revealed by XPS in this study (Table 3). Briefly, Ni^{2+} (O_h) species are formed in both types of structures but the individual species are hard to identify and localize because of their overlapping absorption ranges in the UV-Vis-DRS spectra.

No significant difference between the spectra of Ni/Mg.Al.550.CA and Ni/Mg.Al.550 in the range of 350–800 nm can be found. However, the intensity of the broad signal at 720 nm in the spectrum of Ni/Mg.Al.550.CA (Figure 7b) is lower than that of Ni/Mg.Al.550, indicating less Ni^{2+} species in the domains of bulk NiO-like species which are reducible at low temperature (475 °C, Ni/Mg.Al.550, Figure 5). This suggests that higher dispersion of Ni species can be obtained when CA is added during the preparation. Compared to Ni/Mg.Al.550, a red-shift of the band at around 403 nm can be seen in the Ni/Mg.Al.1000 spectrum (Figure 7b). This shift toward the position of the corresponding intense signal of Ni/MgO illustrates the behavior of the NiO-MgO solid solution. Such a phase formation might be in accordance with the blue-shift of the CT band of the NiO lattice in this sample, displaying the higher stability of the Ni species (Figure 6).


Figure 7. Magnification of complete UV-Vis-DRS spectrum (Figure 6) for supported Ni catalysts and NiO to (**a**) 300-800 nm and (**b**) from 450–800 nm regions.

2.2. Catalyst Performance in the DRM Reaction

Blank tests were carried out in the absence of catalysts or only with the supports in the inert material bed (not shown). No conversion of the feed gases was observed at the favored conditions. Figure 8 shows the CH_4 and CO_2 conversions in DRM during 8 h on stream over the supported Ni catalysts at 650 °C with various supports. The reaction conditions (650 °C, 1 bar, $CH_4:CO_2 = 1$, WHSV = 85 L/($g_{cat} \times$ h)) were chosen to differentiate the activity of the catalysts. Higher activity can be obtained with Mg.Al supported Ni catalysts compared to the single oxide supported samples. Addition of CA during preparation plays a minor role regarding the activity. In contrast, supporting Ni^{2+} on Mg.Al.1000 causes a deterioration of conversion compared to Ni/Mg.Al.550. The latter catalyst exposed the highest activity with the conversions of CH_4 and CO_2 being very close to the thermodynamic limitations for CH_4 (71%) and CO_2 (82%) [49].

In order to verify such high activity of Ni/Mg.Al.550, additional DRM tests at lower temperature with the same WHSV were investigated. Figure 9 shows the excellent performance of Ni/Mg.Al.550 in comparison with the thermodynamic limitations [49]. The catalyst activates CH_4 and CO_2 already around 500 °C. It should be noted that DRM requires high temperatures to convert the reactants to

syngas. According to the literature, the reaction starts at 350 °C, referred to by the thermodynamic calculations [49,50]. Moreover, remarkable conversions of methane and CO_2 were observed only above 500 °C [13]. Some studies claimed the catalysts to be active in DRM at very low temperature (400 °C [51] or 450 °C [50]). However, in those studies more beneficial conditions for high catalytic activity compared to this study were applied (lower WHSV, higher content of active sites, or usage of noble metals). Therefore, the activity of Ni/Mg.Al.550 in this study is outstanding at low temperature considering its low Ni content and the high WHSV (85 L/($g_{cat} \times$ h)) in comparison with other investigations [3,8,52]. Figure 9 displays the effect of temperature on the H_2/CO ratio. This ratio is always lower than unity at any set reaction temperature, which indicates the occurrence of the reverse water gas shift (RWGS) reaction, lowering H_2 selectivity through the reaction with CO_2 to form CO and H_2O [1]. This reaction plays a more important role at lower temperature due to the thermodynamic equilibrium [1].
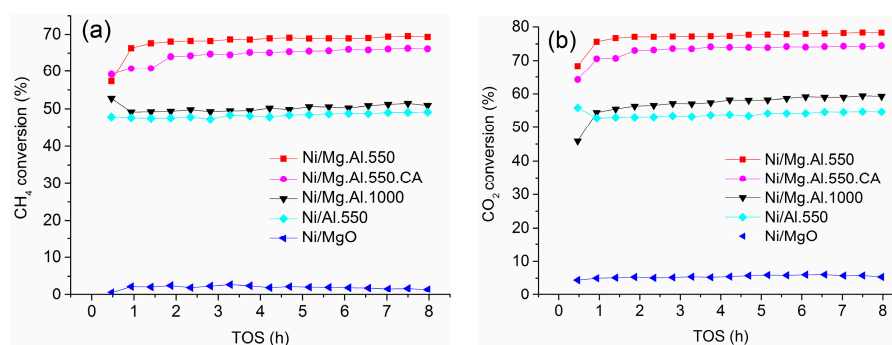

Figure 8. DRM performance of supported Ni catalysts: conversion of (**a**) CH_4 and (**b**) CO_2 (650 °C, 1 bar, CH_4:CO_2 = 1, WHSV = 85 L/($g_{cat} \times$ h), TOS = 8 h).
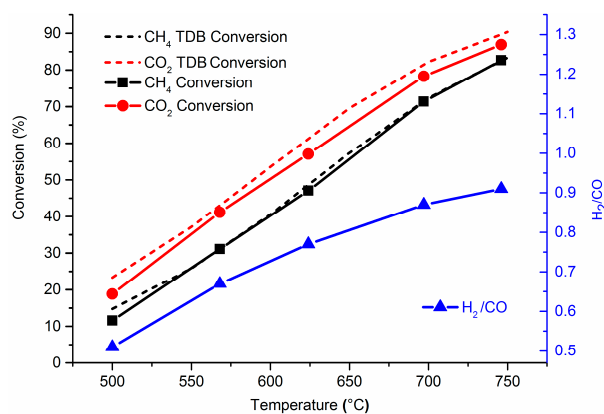
Figure 9. Catalytic performance of Ni/Mg.Al.550 in comparison with the thermodynamic balance (TDB) (1 bar, CH_4:CO_2 = 1, WHSV = 85 L/($g_{cat} \times$ h)). Activity data were collected after 2 h stabilization at each temperature.

The coke deposition behavior in DRM was examined for the Ni catalysts by analyzing the carbon content in the catalysts after 8 h on stream (Figure 10). According to a previous DRM review [49], carbon formation occurs due to methane decomposition (MD) above 550 °C as well as the Boudouard (BD) reaction below 700 °C. Therefore, the reaction temperature in this study was set to 600 °C to study the coking behavior, which is one of the DRM main issues. Carbon deposition during DRM is known to cause catalyst deactivation and reactor plugging [53]. High WHSV (170 L/($g_{cat} \times$ h)) was applied to clearly discriminate the coking resistance among the catalysts. Longer catalyst pre-reduction time (1.5 h) was applied in order to avoid the instant deactivation due to re-oxidation of Ni at a high flowrate of CO_2. The carbon amount found on spent Ni/Mg.Al.550 is higher than that of Ni/Mg.Al.1000 and

Ni/Al.550 (Figure 10). Those amounts appear to be proportional to the conversions in DRM (Figure 8). The addition of CA during the preparation significantly contributes to designing a coking resistant catalyst. Indeed, the carbon amount on Ni/Mg.Al.550.CA is almost 8 times lower than that on Ni/Mg.Al.550 at the same reaction conditions and with similar activity. After 8 h on stream, the carbon content is as low as 0.77 wt % of the sample mass, which is in the range of carbonaceous remainders from the hydrotalcite precursor after calcination. This indicates the high coking resistance of the sample, which is a remarkable result compared to previous research [17,54], especially considering the Ni, Al, and Mg containing catalyst systems.
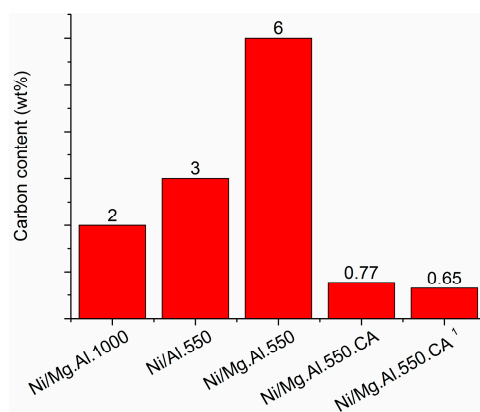
Figure 10. Carbon deposition on spent catalysts after DRM (600 °C, 1 bar, CH_4:CO_2 = 1, WHSV = 170 L/(g_{cat} × h), TOS = 8 h). All the catalysts were in situ pre-reduced for 1.5 h prior to the reaction. [1] Carbon deposition on spent Ni/Mg.Al.550.CA after long term DRM (T = 700 °C, p = 1 bar, CH_4:CO_2 = 1, WHSV = 170 L/(g_{cat} × h), TOS = 60 h).

Long-term DRM was also carried out with Ni/Mg.Al.550.CA (Figure 11). The reaction was implemented at a considerably high WHSV of 170 L/(g_{cat} × h) compared to the literature data [6]. The conversions of CH_4 and CO_2 are very close to the thermodynamic limitations for CH_4 (82%) and CO_2 (86%) [49]. The catalytic performance is almost unchanged after 60 h on-stream, representing high stability of the catalyst in the reaction. At any TOS, the CO_2 conversion is about 8% higher than the CH_4 conversion, illustrating the contribution of the RWGS reaction. The CO selectivity achieves a constant value around 100% (not shown) which is consistent with negligible carbon deposition (<1 wt %) measured after the reaction (Figure 10).
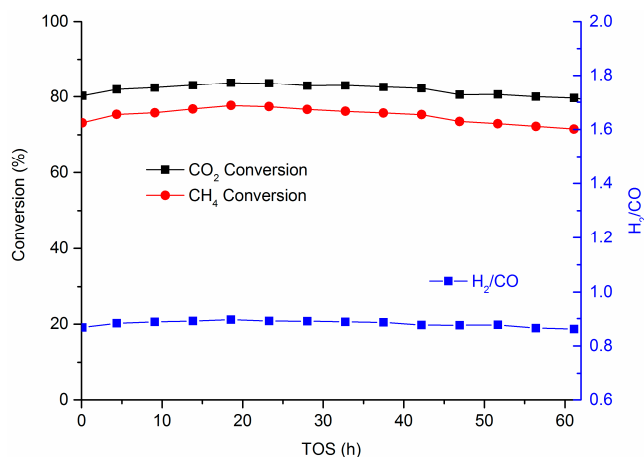
Figure 11. Catalytic performance of Ni/Mg.Al.550.CA in long-term DRM (T = 700 °C, p = 1 bar, CH_4:CO_2 = 1, WHSV = 170 L/(g_{cat} × h)).

3. Discussion

3.1. Activity of Mg.Al Supported Catalysts

Mg.Al supported catalysts show higher activity compared to single oxide supported samples. This is related mainly to their excellent reducibility and Ni enriched surface. This behavior has been also studied elsewhere [20,55], reporting that the coexistence of both Mg and Al in the supports reduces the formation of inactive species (NiO-MgO solid solution, $NiAl_2O_4$ spinel), stabilizes the Ni species on the surface, and subsequently enhances the DRM performance.

Ni/Mg.Al.550 is the most active catalyst for DRM among the studied samples because it possesses a high surface concentration of Ni in combination with the large surface of the support, forming species that are well reduced by H_2. Those active sites are proposed to be Ni^{2+} (O_h) in cooperation with the solid solution of MgO and Al_2O_3 (periclase structure) or surface $NiAl_2O_4$. Such phases are formed and stabilized at high calcination temperature (800 °C), but are still active at high WHSV and low temperature conditions even with low loading of Ni. The modification of such samples by using more severely calcined Mg.Al.1000 or adding CA during impregnation causes poorer reducibility and thus lower CH_4 and CO_2 conversions.

3.2. Coking Resistance and Stability of Mg.Al Supported Catalysts

It is well-known that coking during DRM is related to the large metal particles [4,56]. This is the result of the metal mobility on the surface and the subsequent agglomeration leading to less dispersed particles or clusters [49]. Ni/Mg.Al.550 presents the highest carbon deposition after 8 h on stream (Figure 10). However, the conversion is almost the same, the H_2/CO ratio is constant at 0.78, and the CO selectivity is almost 100% over the complete TOS. Therefore, such carbon deposition can be considered as negligible for catalyst performance. This high coking resistance can also be correlated to the low Ni content and high surface area of the support, by which both the metal and carbon species can be highly dispersed. Such dispersion results in less formation of big Ni particles and lower pore plugging by coke deposition, suppressing fast catalyst deactivation [53].

Ni/Mg.Al.550.CA shows the lowest carbon deposit amount after 8 h and even after 60 h, which is likely to be due to the stable dispersion of Ni species on the support surface. It was suggested above that the Ni/Mg.Al.550.CA sample has a stronger metal-support interaction and less NiO-like domains on the surface, contributing to a better coking resistance of the sample. This strong interaction also contributes to maintaining the catalyst performance in the long-term DRM experiment (Figure 11), by preventing Ni agglomeration and the loss of active sites.

There is another possible explanation for the coke resistance of Ni/Mg.Al.550.CA when comparing the Ni $3p_{3/2}$ BE in the XPS results. The BE values, which are recorded at 856.91 eV and 855.18 eV (Table 3, Figure 12), are assigned to the surface $NiAl_2O_4$ in the Ni/Mg.Al.550 sample and the Ni-Mg-O solid solution in Ni/Mg.Al.550.CA.

Additionally, the surface atom Mg/Al ratio of Ni/Mg.Al.550 (Table 3) exposes an excess amount of Al species on the surface, also suggesting surface $NiAl_2O_4$ formation in Ni/Mg.Al.550 [38]. In contrast, the surface Mg concentration is highest in Ni/Mg.Al.550.CA, revealing the possibility of preferable Ni-Mg interactions on the surface. Our current explanation is that most of the Ni species on the surface of Ni/Mg.Al.550.CA might interact with Mg in the support, providing an effective carbon gasification by CO_2 (reverse Boudouard reaction) and thus coke deposition is suppressed [20], especially at high reaction temperatures (Figure 10). Therefore, Ni/Mg.Al.500.CA may show two beneficial effects that help to suppress coking during DRM: one correlates with the stable physicochemical properties and the other associates with the carbon gasification behavior.
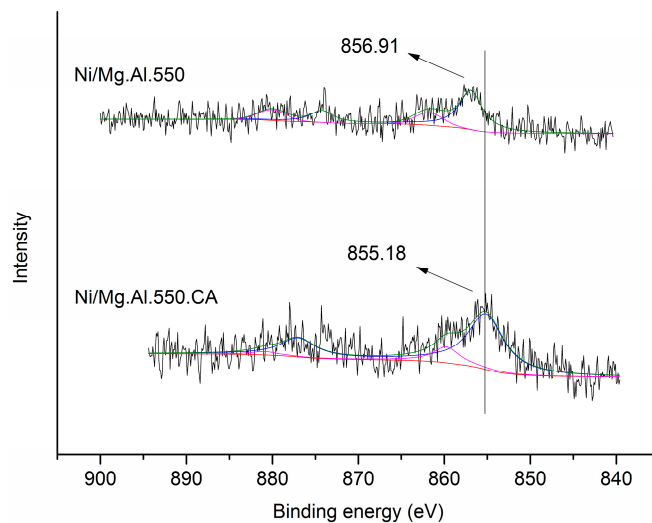
Figure 12. Ni 2p$_{3/2}$ XPS spectra of Ni/Mg.Al.550 and Ni/Mg.Al.550.CA (coloured lines: deconvoluted signals; blue = Ni 2p$_{3/2}$ and Ni 2p$_{1/2}$, magenta = corresponding satellite signals, green = averaged raw data).

4. Materials and Methods

4.1. Catalyst Preparation

Mg-Al mixed oxide (calcined Mg-Al hydrotalcite, Pural MG, Sasol) supported Ni catalysts were prepared by wet impregnation. Ni(NO$_3$)$_2$·6H$_2$O (Carl Roth, Karlsruhe, Germany) was used as the precursor for Ni. The Mg-Al hydrotalcite precursor possesses an Mg/Al ratio = 1.3 (data from ICP-OES and AAS measurement). Prior to impregnation, the precursor samples were calcined at different temperatures (550 °C, 700 °C, 800 °C, 1000 °C) for 6 h in air to obtain the corresponding bare supports which are denoted as Mg.Al.X, in which X represents the support calcination temperature. The calculated amount of Ni precursor was dissolved in deionized water and the solution was stirred for 4 h. The supports were then put into the solution and the slurry was kept stirring at 60 °C for 15 h. Water was removed by a rotary evaporator and the samples were dried overnight and calcined at 400 °C for 3 h and then at 800 °C for 6 h, both in air. The final catalysts are symbolized as Ni/Mg.Al.X. Citric acid (CA) was added simultaneously to the Ni precursor solution in the case of Ni/Mg.Al.550.CA preparation to study the influence of the chelating agent on impregnation. The nominal content of Ni in all supported Ni-containing catalysts was 2.5 wt %. Other materials were used as reference materials; those are MgO (FLUKA) and Al$_2$O$_3$ (boehmite calcined at 550 °C, Pural SB, Sasol) as well as their corresponding 2.5 wt % Ni samples (Ni/MgO and Ni/Al.550). One Mg-Al hydrotalcite sample was calcined first at 550 °C for 6 h and then at 800 °C for 6 h to obtain a material that provides properties similar to the support of Ni/Mg.Al.550.CA and Ni/Mg.Al.550, because those catalysts were calcined at 800 °C. That material is denoted as Mg.Al.550.800. Pure NiO was prepared by calcining Ni(NO$_3$)$_2$·6H$_2$O (Alfa Aesar) at 800 °C.

4.2. Catalyst Characterization

The metal (Ni, Mg, Al) contents of the samples were determined by inductively coupled plasma-optical emission spectroscopy (ICP-OES) using a 715-ES device (Varian, Inc., Palo Alto, CA, USA) and atomic adsorption spectroscopy (AAS) using an Analyst 300 apparatus (PerkinElmer, Inc., Waltham, MA, USA), respectively. The carbon deposition on spent catalysts was analyzed using a Truespace CHNS analyzer (LECO Corporation, Saint Joseph, MI, USA). After the reaction, the reactor was cooled to room temperature under Ar flow. Then the spent catalysts were separated from the inert material by sieving and transferred to the CHNS device.

The nitrogen physisorption method was used to calculate the specific surface area and pore volume distribution according to the BET theory and BJH calculation, respectively. The measurements were performed on a Micromeritics ASAP 2010 apparatus (Micromeritics GmbH, Aachen, Germany) at −196 °C. The samples were degassed at 200 °C in vacuum for 4 h before the analysis.

The XRD powder patterns were recorded either on a Panalytical X'Pert diffractometer (Almelo, The Netherlands) equipped with a X'celerator detector or on a Panalytical Empyrean diffractometer (Almelo, The Netherlands) equipped with a PIXcel 3D detector system using Cu Kα_1/α_2 radiation (40 kV, 40 mA) in both cases. Cu beta-radiation was excluded by using a nickel filter foil. The Cu K alpha2 radiation contribution was removed arithmetically using the Panalytical HighScore Plus software package (V. 3.0e, Panalytical, Almelo, The Netherlands). The peak positions and profile were fitted with the Pseudo-Voigt function using the WinXPow software package (V3.0.2, Stoe, Darmstadt, Germany). Phase identification was done by using the PDF-2 database of the International Center of Diffraction Data (ICDD).

XPS measurements were carried out with a VG ESCALAB 220iXL instrument (Thermo Fisher Scientific, Inc., Waltham, MA, USA) with monochromatic AlKα radiation (E = 1486.68 eV). The peak areas were determined after background subtraction and fitting with Gaussian-Lorentzian curves. The amount of each component in the near-surface region can be calculated based on these peak areas with division by the element-specific Scofield factor and the transmission function of the spectrometer.

For the H_2-TPR experiments, the measurement was done using a Autochem II 2920 instrument (Micromeritics, Aachen, Germany). A 300 mg sample was loaded into a U-shaped quartz reactor and heated from room temperature (RT) to 400 °C at 20 K/min in 5% O_2/He (50 mL/min) for 30 min at 400 °C, and was then cooled to RT and the sample was flushed with Ar. The TPR run was carried out from RT to 1000 °C in a 5% H_2/Ar flow (50 mL/min) with a heating rate of 10 K/min and was then held at the final temperature for 30 min before being cooled to RT. The hydrogen consumption peaks, indicating the reduction, were recorded using a TCD detector. The amount of hydrogen consumed was calculated based on the peak areas.

UV-Vis-DR spectra were measured over the wavelength range of 200–800 nm using a Cary 5000 spectrometer (Agilent Technologies, Petaling Jaya, Malaysia) equipped with a diffuse reflectance accessory (praying mantis, Harrick). In normal experiments, $BaSO_4$ is used as a reference white standard and dilute material for pure NiO measurement because of its high Ni content.

4.3. Catalytic Tests

DRM was carried out in a fixed bed continuous flow quartz reactor (ambient pressure, WHSV = 85 or 170 L/(g_{cat} × h); T = 500–700 °C). All volumetric flow rates given in this study are related to 25 °C and atmospheric pressure. After in situ pre-reduction in H_2 (700 °C, 100% H_2, 50 mL/min) for 1 h (used in the activity and stability tests) or 1.5 h (used for the coking test), the temperature was adjusted and maintained for 8 or 72 h and the reactant mixture (45 vol % CH_4, 45 vol % CO_2, 10 vol % He) was fed to the reactor. Helium was used as the internal standard for volume change estimation in the reaction. The gas compositions were then analyzed by an on-line Agilent 6890 gas chromatograph (Agilent Technologies, Santa Clara, CA, USA) equipped with a flame ionization detector (HP Plot Q capillary, 15 m × 0.53 mm × 40 μm) and a thermal conductivity detector (Carboxene packed, 4.572 m × 3.175 mm) for the analysis of hydrocarbons and permanent gases, respectively. Pure components were used as references for peak identification and calibration. Carbon balances were calculated from the gas products reaching more than 95% in this work. Conversions (X) and the H_2/CO ratio were calculated using the formulas given below:

$$X_{CH_4} \ (\%) = \frac{\text{moles of converted } CH_4 \times 100\%}{\text{moles of } CH_4 \text{ in feed}} \tag{4}$$

$$X_{CO_2} \ (\%) = \frac{\text{moles of } CO_2 \text{ converted} \times 100\%}{\text{moles of } CO_2 \text{ in feed}} \tag{5}$$

$$H_2/CO \text{ ratio} = \frac{\text{moles of } H_2 \text{ produced}}{\text{moles of CO produced}} \tag{6}$$

Author Contributions: Q.L.M.H., A.M., and U.A. conceived and designed the experiments; Q.L.M.H. performed the experiments and analyzed the data; H.A. performed the TPR measurements; H.L. and M.S. performed the XRD measurements; G.A. and J.R. performed the XPS measurements; H.T.V. analyzed the UV-Vis-DRS data; Q.L.M.H. and U.A. wrote the paper.

Conflicts of Interest: The authors declare no conflict of interest.

References

1. Havran, V.; Duduković, M.P.; Lo, C.S. Conversion of Methane and Carbon Dioxide to Higher Value Products. *Ind. Eng. Chem. Res.* **2011**, *50*, 7089–7100. [CrossRef]
2. Rostrupnielsen, J.R.; Hansen, J.H.B. CO_2-Reforming of Methane over Transition Metals. *J. Catal.* **1993**, *144*, 38–49. [CrossRef]
3. Fan, M.-S.; Abdullah, A.Z.; Bhatia, S. Catalytic Technology for Carbon Dioxide Reforming of Methane to Synthesis Gas. *Chemcatchem* **2009**, *1*, 192–208. [CrossRef]
4. Bradford, M.C.J.; Vannice, M.A. CO_2 Reforming of CH_4. *Catal. Rev.* **1999**, *41*, 1–42. [CrossRef]
5. Wurzel, T.; Malcus, S.; Mleczko, L. Reaction engineering investigations of CO_2 reforming in a fluidized-bed reactor. *Chem. Eng. Sci.* **2000**, *55*, 3955–3966. [CrossRef]
6. Oyama, S.T.; Hacarlioglu, P.; Gu, Y.; Lee, D. Dry reforming of methane has no future for hydrogen production: Comparison with steam reforming at high pressure in standard and membrane reactors. *Int. J. Hydrog. Energy* **2012**, *37*, 10444–10450. [CrossRef]
7. Albarazi, A.; Gálvez, M.E.; Da Costa, P. Synthesis strategies of ceria–zirconia doped Ni/SBA-15 catalysts for methane dry reforming. *Catal. Commun.* **2015**, *59*, 108–112. [CrossRef]
8. Usman, M.; Wan Daud, W.M.A.; Abbas, H.F. Dry reforming of methane: Influence of process parameters—A review. *Renew. Sustain. Energy Rev.* **2015**, *45*, 710–744. [CrossRef]
9. Paksoy, A.I.; Caglayan, B.S.; Aksoylu, A.E. A study on characterization and methane dry reforming performance of Co–Ce/ZrO_2 catalyst. *Appl. Catal. B Environ.* **2015**, *168–169*, 164–174. [CrossRef]
10. Yu, M.; Zhu, Y.-A.; Lu, Y.; Tong, G.; Zhu, K.; Zhou, X. The promoting role of Ag in Ni-CeO_2 catalyzed CH_4-CO_2 dry reforming reaction. *Appl. Catal. B Environ.* **2015**, *165*, 43–56. [CrossRef]
11. Ma, J.; Sun, N.; Zhang, X.; Zhao, N.; Xiao, F.; Wei, W.; Sun, Y. A short review of catalysis for CO_2 conversion. *Catal. Today* **2009**, *148*, 221–231. [CrossRef]
12. Liu, C.-J.; Ye, J.; Jiang, J.; Pan, Y. Progresses in the Preparation of Coke Resistant Ni-based Catalyst for Steam and CO_2 Reforming of Methane. *ChemCatChem* **2011**, *3*, 529–541. [CrossRef]
13. Gao, J.; Hou, Z.; Lou, H.; Zheng, X. Chapter 7—Dry (CO_2) Reforming. In *Fuel Cells: Technologies for Fuel Processing*; Elsevier: Amsterdam, The Netherlands, 2011; pp. 191–221.
14. Edwards, J.H.; Maitra, A.M. The chemistry of methane reforming with carbon dioxide and its current and potential applications. *Fuel Process. Technol.* **1995**, *42*, 269–289. [CrossRef]
15. Tang, S.B.; Qiu, F.L.; Lu, S.J. Effect of supports on the carbon deposition of nickel catalysts for methane reforming with CO_2. *Catal. Today* **1995**, *24*, 253–255. [CrossRef]
16. Roh, H.-S.; Jun, K.-W. Carbon Dioxide Reforming of Methane over Ni Catalysts Supported on Al_2O_3 Modified with La_2O_3, MgO, and CaO. *Catal. Surv. Asia* **2008**, *12*, 239–252. [CrossRef]
17. Guo, J.; Lou, H.; Zhao, H.; Chai, D.; Zheng, X. Dry reforming of methane over nickel catalysts supported on magnesium aluminate spinels. *Appl. Catal. A Gen.* **2004**, *273*, 75–82. [CrossRef]
18. Habibi, N.; Arandiyan, H.; Rezaei, M. Mesoporous $MgO·Al_2O_3$ nanopowder-supported meso-macroporous nickel catalysts: A new path to high-performance biogas reforming for syngas. *RSC Adv.* **2016**, *6*, 29576–29585. [CrossRef]

19. Abdollahifar, M.; Haghighi, M.; Babaluo, A.A.; Talkhoncheh, S.K. Sono-synthesis and characterization of bimetallic Ni–Co/Al$_2$O$_3$–MgO nanocatalyst: Effects of metal content on catalytic properties and activity for hydrogen production via CO$_2$ reforming of CH$_4$. *Ultrason. Sonochem.* **2016**, *31*, 173–183. [CrossRef] [PubMed]

20. García-Diéguez, M.; Herrera, C.; Larrubia, M.Á.; Alemany, L.J. CO$_2$-reforming of natural gas components over a highly stable and selective NiMg/Al$_2$O$_3$ nanocatalyst. *Catal. Today* **2012**, *197*, 50–57. [CrossRef]

21. Zhang, J.; Wang, H.; Dalai, A.K. Effects of metal content on activity and stability of Ni-Co bimetallic catalysts for CO$_2$ reforming of CH$_4$. *Appl. Catal. A Gen.* **2008**, *339*, 121–129. [CrossRef]

22. Kim, J.-H.; Suh, D.J.; Park, T.-J.; Kim, K.-L. Effect of metal particle size on coking during CO$_2$ reforming of CH$_4$ over Ni–alumina aerogel catalysts. *Appl. Catal. A Gen.* **2000**, *197*, 191–200. [CrossRef]

23. Suárez-Toriello, V.A.; Santolalla-Vargas, C.E.; de los Reyes, J.A.; Vázquez-Zavala, A.; Vrinat, M.; Geantet, C. Influence of the solution pH in impregnation with citric acid and activity of Ni/W/Al$_2$O$_3$ catalysts. *J. Mol. Catal. Chem.* **2015**, *404–405*, 36–46. [CrossRef]

24. Van Dillen, A.J.; Terörde, R.J.A.M.; Lensveld, D.J.; Geus, J.W.; de Jong, K.P. Synthesis of supported catalysts by impregnation and drying using aqueous chelated metal complexes. *J. Catal.* **2003**, *216*, 257–264. [CrossRef]

25. Prescott, H.A.; Li, Z.-J.; Kemnitz, E.; Trunschke, A.; Deutsch, J.; Lieske, H.; Auroux, A. Application of calcined Mg-Al hydrotalcites for Michael additions: An investigation of catalytic activity and acid-base properties. *J. Catal.* **2005**, *234*, 119–130. [CrossRef]

26. Ono, Y.; Hattori, H. Preparation and Catalytic Properties of Solid Base Catalysts—II. Specific Materials for Solid Bases. In *Solid Base Catalysis*; Springer: Berlin/Heidelberg, Germany, 2011; pp. 157–218.

27. Kumar, P.A.; Reddy, M.P.; Hyun-Sook, B.; Phil, H.H. Influence of Mg Addition on the Catalytic Activity of Alumina Supported Ag for C$_3$H$_6$-SCR of NO. *Catal. Lett.* **2009**, *131*, 85–97. [CrossRef]

28. Stanimirova, T.; Vergilov, I.; Kirov, G.; Petrova, N. Thermal decomposition products of hydrotalcite-like compounds: Low-temperature metaphases. *J. Mater. Sci.* **1999**, *34*, 4153–4161. [CrossRef]

29. Takehira, K.; Kawabata, T.; Shishido, T.; Murakami, K.; Ohi, T.; Shoro, D.; Honda, M.; Takaki, K. Mechanism of reconstitution of hydrotalcite leading to eggshell-type Ni loading on MgAl mixed oxide. *J. Catal.* **2005**, *231*, 92–104. [CrossRef]

30. Escobar, J.; De Los Reyes, J.A.; Viveros, T. Nickel on TiO$_2$-modified Al$_2$O$_3$ sol–gel oxides: Effect of synthesis parameters on the supported phase properties. *Appl. Catal. A Gen.* **2003**, *253*, 151–163. [CrossRef]

31. Damyanova, S.; Pawelec, B.; Arishtirova, K.; Fierro, J.L.G. Ni-based catalysts for reforming of methane with CO$_2$. *Int. J. Hydrog. Energy* **2012**, *37*, 15966–15975. [CrossRef]

32. Jafarbegloo, M.; Tarlani, A.; Mesbah, A.W.; Muzart, J.; Sahebdelfar, S. NiO–MgO Solid Solution Prepared by Sol–Gel Method as Precursor for Ni/MgO Methane Dry Reforming Catalyst: Effect of Calcination Temperature on Catalytic Performance. *Catal. Lett.* **2016**, *146*, 238–248. [CrossRef]

33. Li, C.; Chen, Y.-W. Temperature-programmed-reduction studies of nickel oxide/alumina catalysts: Effects of the preparation method. *Thermochim. Acta* **1995**, *256*, 457–465. [CrossRef]

34. Rogers, J.L.; Mangarella, M.C.; D'Amico, A.D.; Gallagher, J.R.; Dutzer, M.R.; Stavitski, E.; Miller, J.T.; Sievers, C. Differences in the Nature of Active Sites for Methane Dry Reforming and Methane Steam Reforming over Nickel Aluminate Catalysts. *ACS Catal.* **2016**, *6*, 5873–5886. [CrossRef]

35. Lucrédio, A.F.; Bellido, J.D.A.; Assaf, E.M. Effects of adding La and Ce to hydrotalcite-type Ni/Mg/Al catalyst precursors on ethanol steam reforming reactions. *Appl. Catal. A Gen.* **2010**, *388*, 77–85. [CrossRef]

36. Jiang, Z.; Su, J.; Jones, M.O.; Shi, H.; Xiao, T.; Edwards, P.P. Catalytic Partial Oxidation of Methane over Ni-Based Catalysts Derived from Ni-Mg/Al Ternary Hydrotalcites. *Energy Fuels* **2009**, *23*, 1634–1639. [CrossRef]

37. Sánchez-Sánchez, M.C.; Navarro, R.M.; Fierro, J.L.G. Ethanol steam reforming over Ni/M$_x$O$_y$-Al$_2$O$_3$ (M = Ce, La, Zr and Mg) catalysts: Influence of support on the hydrogen production. *Int. J. Hydrog. Energy* **2007**, *32*, 1462–1471. [CrossRef]

38. Özdemir, H.; Öksüzömer, M.A.F.; Gürkaynak, M.A. Effect of the calcination temperature on Ni/MgAl$_2$O$_4$ catalyst structure and catalytic properties for partial oxidation of methane. *Fuel* **2014**, *116*, 63–70. [CrossRef]

39. NIST X-ray Photoelectron Spectroscopy Database: Version 3.4 (Web Version). Available online: http://srdata.nist.gov/xps/ (accessed on 6 February 2017).

40. Cimino, A.; Gazzoli, D.; Indovina, V.; Moretti, G.; Occhiuzzi, M.; Pepe, F. High and low surface area NiO–MgO and CoO–MgO solid solutions: A study of XPS surface composition and CO oxidation activity. *Top. Catal.* **1999**, *8*, 171–178. [CrossRef]

41. Ruckenstein, E.; Hu, Y.H. Methane partial oxidation over NiO/MgO solid solution catalysts. *Appl. Catal. A Gen.* **1999**, *183*, 85–92. [CrossRef]

42. Scheffer, B.; Heijeinga, J.J.; Moulijn, J.A. An electron spectroscopy and X-ray diffraction study of nickel oxide/alumina and nickel-oxide-tungsten trioxide/alumina catalysts. *J. Phys. Chem.* **1987**, *91*, 4752–4759. [CrossRef]

43. Boukha, Z.; Jiménez-González, C.; de Rivas, B.; González-Velasco, J.R.; Gutiérrez-Ortiz, J.I.; López-Fonseca, R. Synthesis, characterisation and performance evaluation of spinel-derived Ni/Al$_2$O$_3$ catalysts for various methane reforming reactions. *Appl. Catal. B Environ.* **2014**, *158–159*, 190–201. [CrossRef]

44. Heracleous, E.; Lee, A.F.; Wilson, K.; Lemonidou, A.A. Investigation of Ni-based alumina-supported catalysts for the oxidative dehydrogenation of ethane to ethylene: Structural characterization and reactivity studies. *J. Catal.* **2005**, *231*, 159–171. [CrossRef]

45. Jiménez-González, C.; Boukha, Z.; de Rivas, B.; González-Velasco, J.R.; Gutiérrez-Ortiz, J.I.; López-Fonseca, R. Behavior of Coprecipitated NiAl$_2$O$_4$/Al$_2$O$_3$ Catalysts for Low-Temperature Methane Steam Reforming. *Energy Fuels* **2014**, *28*, 7109–7121. [CrossRef]

46. Skoufa, Z.; Xantri, G.; Heracleous, E.; Lemonidou, A.A. A study of Ni–Al–O mixed oxides as catalysts for the oxidative conversion of ethane to ethylene. *Appl. Catal. A Gen.* **2014**, *471*, 107–117. [CrossRef]

47. Zecchina, A.; Spoto, G.; Coluccia, S.; Guglielminotti, E. Spectroscopic study of the adsorption of carbon monoxide on solid solutions of nickel oxide and magnesium oxide. Part 1—Standard samples. *J. Chem. Soc. Faraday Trans.* **1984**, *80*, 1875–1889. [CrossRef]

48. Lucrédio, A.F.; Jerkiewickz, G.; Assaf, E.M. Nickel catalysts promoted with cerium and lanthanum to reduce carbon formation in partial oxidation of methane reactions. *Appl. Catal. A Gen.* **2007**, *333*, 90–95. [CrossRef]

49. Pakhare, D.; Spivey, J. A review of dry (CO$_2$) reforming of methane over noble metal catalysts. *Chem. Soc. Rev.* **2014**, *43*, 7813–7837. [CrossRef] [PubMed]

50. Elsayed, N.H.; Roberts, N.R.M.; Joseph, B.; Kuhn, J.N. Low temperature dry reforming of methane over Pt–Ni–Mg/ceria–zirconia catalysts. *Appl. Catal. B Environ.* **2015**, *179*, 213–219. [CrossRef]

51. Sokolov, S.; Kondratenko, E.V.; Pohl, M.-M.; Barkschat, A.; Rodemerck, U. Stable low-temperature dry reforming of methane over mesoporous La$_2$O$_3$-ZrO$_2$ supported Ni catalyst. *Appl. Catal. B Environ.* **2012**, *113–114*, 19–30. [CrossRef]

52. Lavoie, J.-M. Review on dry reforming of methane, a potentially more environmentally-friendly approach to the increasing natural gas exploitation. *Front. Chem.* **2014**, *2*, 81. [CrossRef] [PubMed]

53. Newson, E. Catalyst Deactivation Due to Pore-Plugging by Reaction Products. *Ind. Eng. Chem. Proc. Des. Dev.* **1975**, *14*, 27–33. [CrossRef]

54. Muraza, O.; Galadima, A. A review on coke management during dry reforming of methane. *Int. J. Energy Res.* **2015**, *39*, 1196–1216. [CrossRef]

55. Alipour, Z.; Rezaei, M.; Meshkani, F. Effect of alkaline earth promoters (MgO, CaO, and BaO) on the activity and coke formation of Ni catalysts supported on nanocrystalline Al$_2$O$_3$ in dry reforming of methane. *J. Korean Ind. Eng. Chem.* **2014**, *20*, 2858–2863. [CrossRef]

56. York, A.P.E.; Xiao, T.-C.; Green, M.L.H.; Claridge, J.B. Methane Oxyforming for Synthesis Gas Production. *Catal. Rev.* **2007**, *49*, 511–560. [CrossRef]